Relaxation of 2D Turbulence to Vortex Crystals

K. S. Fine, A. C. Cass, W. G. Flynn,* and C. F. Driscoll
Physics Department and Institute for Pure and Applied Physical Sciences, University of California at San Diego, La Jolla, California 92093
(Received 19 April 1995)

Two-dimensional turbulence normally relaxes through vortex merger and filamentation, with energy flowing to large scales and enstrophy dissipated on fine scales. Experiments on magnetized electron columns show that this relaxation can be arrested by spontaneous "cooling" of the chaotic vortex motions, leading to regular lattices of vortices within a uniform background of weaker vorticity.

PACS numbers: 47.27.Jv, 47.32.Cc, 52.25.Wz, 52.35.Ra

In the relaxation of turbulence in nearly inviscid 2D flows, energy flows to long wavelengths, while enstrophy is dissipated on fine scales [1], leading to inviscid invariants that are "fragile" or "robust" in the presence of weak viscosity [2]. Relaxed states can be predicted based on maximization of entropy [3,4] or minimization of enstrophy [5], and surprising agreement with the minimum enstrophy states has been found in experiments in some parameter regimes [6].

However, experiments [7] and computation [8] demonstrate that long-lived nonlinear vortices often dominate the evolution, arising even from structureless initial conditions. The vortices seem to move chaotically due to mutual advection, resulting in pairwise merger events and the formation of filamentary structures. A scaling theory of relaxation [9,10] based on mergers with conservation of energy and maximum vorticity predicts power law dependences of vortex properties, e.g., number of vortices $N_v \propto t^{-\xi}$, and simulations have suggested $\xi = 0.75$. Contour dynamics calculations suggest more complicated merger and filamentation events, and give different scaling exponents [11]. Electrolyte experiments with strong dissipation have shown a range of exponents [12].

Here, we observe the free relaxation of turbulence in magnetized electron columns, which evolve as near-ideal 2D fluids. We find that the relaxation can be arrested by the formation of vortex crystals: for some initial conditions, the chaotic motion of the vortices is "cooled," no further merger events occur, and the vortices form a rigidly rotating lattice within a uniform background of vorticity. The vortex crystal state is observed to persist for up to 10^4 turnover times, until dissipation acts on the individual vortices. Similar geometric patterns of point vortices have been seen in rotating superfluids, where friction arises from interaction with normal fluid [13].

In our case, the cooling appears to be a 2D fluid process, showing little length dependence, and occurring in a few turnover times. We speculate that the cooling is caused by the interchange of energy between the motion of individual vortices and the background vorticity [14], made irreversible by fine-scale dissipation or mode damping [15].

Figure 1 shows the experimental device with the imaging diagnostic. Electrons from a spiral tungsten filament are trapped in a series of conducting cylinders (radius $R_w = 3.5$ cm) enclosed in a vacuum chamber ($\lesssim 10^{-9}$ torr). The electrons are contained axially by negative voltages (-50 V) on the two end cylinders, and confined radially by a uniform axial magnetic field ($B_z = 4$ kG), resulting in a confinement time of about 100 sec. The trapped electron column typically has density $n \leq 7 \times 10^6$ cm^{-3}, radius $R_p \sim 1.5$ cm, and axial length $L_p \sim 50$ cm. The electrons have average kinetic energy $kT \approx 1$ eV and are effectively collisionless, with mean free path $\lambda_{ee} \approx 3$ km. Individual electrons bounce rapidly axially ($f_z \equiv \bar{v}/2L_p \approx 0.4$ MHz), averaging over any z variations. Kinetic energy perpendicular to B_z is bound up in cyclotron orbits, which are fast ($f_c \approx 11$ GHz) and small ($r_c \approx 5$ μm) enough to be ignorable.

Electric fields then cause the electron guiding centers to $\mathbf{E} \times \mathbf{B}$ drift across the magnetic field as an effectively incompressible fluid. This (r, θ) flow of the electrons is described by the 2D drift-Poisson equations [15,16],

$$\frac{\partial n}{\partial t} + \mathbf{v} \cdot \nabla n = 0, \qquad \mathbf{v} = -\frac{c}{B_z} \nabla \phi \times \hat{\mathbf{z}},$$
$$\nabla^2 \phi = 4\pi e n, \tag{1}$$

where $\mathbf{v}(r, \theta)$ is the drift velocity and $-e$ is the electron charge. The drifts are predominantly azimuthal, with bulk rotation time $\tau_R \approx 170$ μs. The electron density $n(r, \theta)$ is proportional to the flow vorticity $\zeta(r, \theta)$, since $\zeta \equiv \hat{\mathbf{z}} \cdot (\nabla \times \mathbf{v}) = (4\pi ec/B_z)n$. The electrostatic potential $\phi(r, \theta)$ is proportional to the stream function, and the nonzero $\partial\phi/\partial r$ at the wall gives a true free-slip boundary

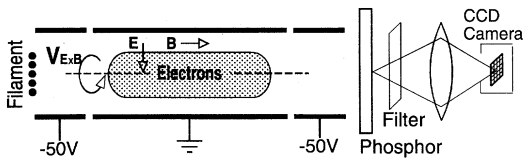

FIG. 1. The cylindrical experimental apparatus with phosphor screen/CCD camera diagnostic.

0031-9007/95/75(18)/3277(4)$06.00

condition. Equations (1) are isomorphic to the Euler equation that governs 2D inviscid incompressible fluids. For fine spatial scales or long times, plasma "viscous" [17] or diffusive effects [18] not contained in Eqs. (1) become significant; however, these are *not* in general modeled by the Navier-Stokes equation.

At any desired time, the z-integrated electron density $n(r,\theta,t)$ is measured (destructively) by dumping the electrons axially onto a phosphor screen, from which the luminescence is imaged by a low-noise 512×512 pixel CCD camera. The shot-to-shot variations in the initial profiles are small, i.e., $\delta n/n \lesssim 10^{-2}$, so the time evolution can be inferred from a sequence of shots with differing hold times.

For the experiments described here, we initially trap a highly filamented electron density distribution from the spiral electron source, rather than a smooth profile as studied previously [6]. Many individual vortices then form due to local Kelvin-Helmholtz instabilities, and this turbulent state evolves and relaxes by chaotic vortex advection and mergers.

Figure 2 shows the measured vorticity $\zeta(r,\theta,t)$ at five times for two slightly different initial conditions, varied by changing the filament bias voltages. The upper sequence forms vortex crystals, whereas the lower sequence relaxes rapidly to a monotonically decreasing profile. The vortex crystal states consist of 5–11 individual vortices each with vorticity 4–6 times the background vorticity, arranged in a lattice pattern that rotates with the background. In plasma terms, rods of enhanced electron density ($n \sim 7 \times 10^6$ cm^{-3}) are maintaining self-coherence and positions relative to each other for several seconds, while $\mathbf{E} \times \mathbf{B}$ drifting with a diffuse background ($n_B \sim 2 \times 10^6$ cm^{-3}). Vortex crystal states are repeatably observed over a range of filament bias voltages, but the characteristics of the initial $n(r,\theta)$ required for these states are not yet understood.

Figure 3 shows the number of distinct vortices N_v, the circulation in these vortices $\sum \Gamma_v$, and the average vortex radius $\langle r_v \rangle$ for the two sequences after distinct vortices form. The vortex counting algorithm is essentially that of McWilliams [19] without the exclusion of elongated structures. In both sequences, the unstable filamentary initial condition forms $N_v = 50-100$ vortices of roughly equal circulation, after which N_v initially decreases as $N_v \sim t^{-\xi}$, with $\xi \approx 1$. This relaxation is generally consistent with the scaling of Refs. [9]; the observed ξ range from 0.4 to 1.1 as the initial conditions are varied, with 0.8 being commonly observed. Here, the merger, filamentation, and diffusion results in a decrease in the discrete vortex circulation, roughly as $\sum \Gamma_v \sim t^{-0.6}$ in Fig. 3.

In the evolution of the top sequence in Fig. 2, the relaxation is arrested by the "cooling" of the chaotic vortex motions, with formation of vortex crystals by $10\tau_R$. The diamonds in Fig. 3 show that 8 to 10 distinct vortices survive for about $10^4\tau_R$. When the vortices all have about the same circulation, the patterns are quite regular, as seen at $600\tau_R$ in Fig. 2. After $10^4\tau_R$, N_v decreases to 1 as the individual vortices decay away in place. Other experimental images show that as N_v decreases, the remaining vortices readjust to a new rigidly rotating, symmetrically spaced pattern.

The measured integral quantities, shown in Fig. 4, are consistent with 2D inviscid motion on large scales and dissipation on fine scales. From the measured $n(r,\theta)$ we calculate the number of electrons (per unit length) $N_L \equiv \int d^2\mathbf{r}\, n$, or fluid circulation $\Gamma_{\rm tot} = (4\pi ec/B)N_L$; the canonical angular momentum (fluid angular impulse) $P_\theta \equiv R_w^{-4} \int d^2\mathbf{r}\, r^2 n/n_0$; the electrostatic energy (fluid kinetic energy) $H_\phi \equiv -\frac{1}{2}R_w^{-2} \int d^2\mathbf{r}(\phi/\phi_0)(n/n_0)$; and the enstrophy $Z_2 = \frac{1}{2}R_w^{-2} \int d^2\mathbf{r}(n/n_0)^2$. Here, the characteristic density is $n_0 \equiv N_L/R_w^2$, and the characteristic potential is $\phi_0 \equiv eN_L$.

Experimentally, the circulation, angular momentum, and energy are robust invariants. The circulation shows systematic variations of 10%, probably due to slow variation of the filament emission and slow ionization of background gas when $t \gtrsim 0.1$ sec. This variation of $\Gamma_{\rm tot}$ does not strongly affect P_θ or H_ϕ, since they are scaled by n_0, although the 5% rise in P_θ at late times indicates

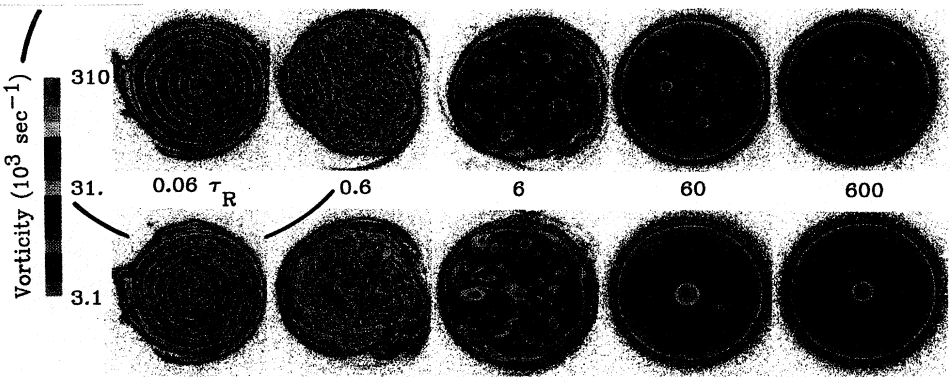

FIG. 2(color). Images of vorticity at five times for two sequences from similar initial conditions. The black arcs indicate the wall radius.

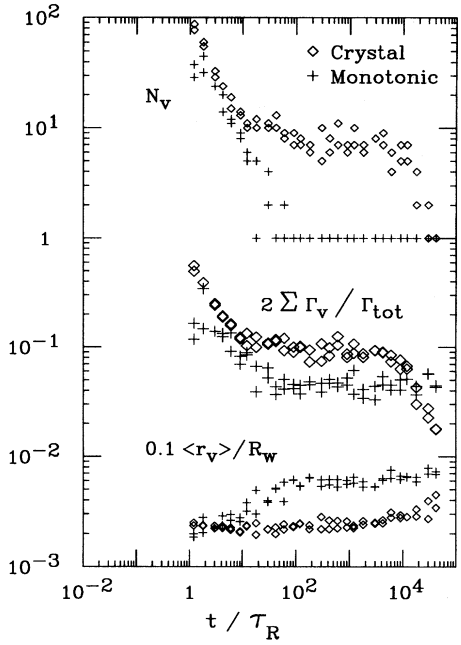

FIG. 3. Evolution of number of vortices, vortex circulation, and average vortex size for the two sequences.

a slightly broader column. The maximum vorticity ζ_{max} shows a 30% increase for the crystals sequence, but no significant change for the monotonic sequence. The reason for this increase is not understood; it may be due to filamentary structures at $t = 0$ that are smaller than the pixel size. In contrast, the enstrophy Z_2 is a "fragile" invariant, and initially decays a factor of 2 in both sequences. For the crystals sequence, Z_2 is constant from $10\tau_R$ until $10^4\tau_R$, at which time the individual vortices decay in place.

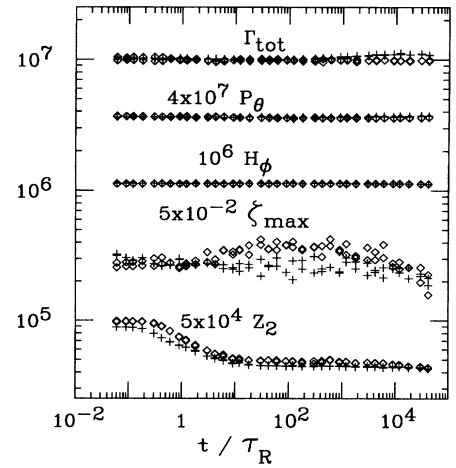

FIG. 4. Evolution of the robust invariants of total circulation, angular momentum, and energy; the maximum observed vorticity; and the fragile enstrophy invariant for the two sequences.

Reduction of the chaotic advective motions of the individual vortices is required to form the vortex crystal states. This "cooling" is shown in Fig. 5. Here, the average magnitude of the random velocities of the individual vortices, $|\delta V|$, is relative to the rotating frame in which the mean discrete vortex velocity is zero. The velocities are obtained from the potential $\phi(r, \theta)$ calculated from the measured $n(r, \theta)$ and boundary conditions $\phi(R_w, \theta) = 0$.

The measured $|\delta V|$ decreases a factor of 6 between $2\tau_R$ and $100\tau_R$ for the crystal's sequence, whereas only slight cooling is seen before $N_v = 1$ (and $|\delta V| = 0$ by definition) for the monotonic sequence. The residual $|\delta V|$ for $t \geq 100\tau_R$ may indicate incomplete cooling, measurement noise, or systematic errors such as uncertainty in the position of the trap axis. We note that the magnitude of $|\delta V|$ expected without cooling would scale as $(\sum \Gamma_v)^1$ and $(N_v)^{-1/2}$, and these two dependencies would essentially cancel, since $N_v \sim t^{-1}$ and $\sum \Gamma \sim t^{-0.6}$.

We believe this cooling and cessation of relaxation through mergers is a near-inviscid 2D fluid effect, i.e., independent of the details of the fine-scale dissipation. However, two essential characteristics of this system are the nonzero total circulation and the boundary of the vorticity patch, effects that may not be present in other systems. It appears that the vortex cooling occurs due to an interaction between the individual vortices and the boundary of the background vorticity. A weak interaction would be described as the excitation of surface waves on the background, and these waves could be damped by direct or beat-wave spatial Landau damping [15]. For strong interactions and short wavelengths, this would correspond to entrainment and mixing of low vorticity regions from the edge of the column. Some of the experimental images suggest this latter process, and it has been clearly observed in 2D vortex-in-cell simulations by one of the authors [14]. A similar process may cause negative (relative) vorticity "holes" to become symmetrically situated, as observed in previous experiments [20].

Figure 6 shows a selection of the symmetric crystal patterns that have been observed. Apparently, there are

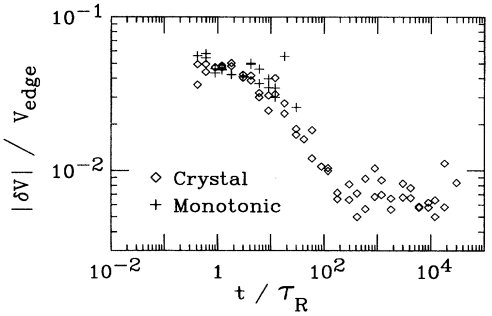

FIG. 5. Evolution of the average chaotic velocity $|\delta V|$ of the vortices for the two sequences, normalized by $V_{edge} \equiv 2\pi R_p/\tau_R = 5.5 \times 10^4$ cm/sec.

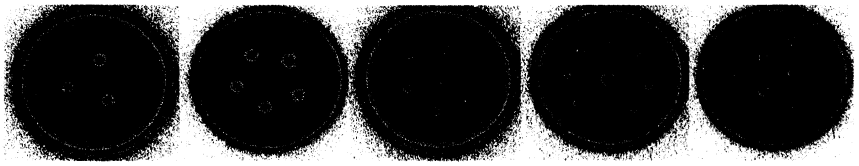

FIG. 6(color). Selection of vortex crystal patterns obtained from initial conditions similar to those of Fig. 2.

many different "meta-equilibria" to which the system can evolve under near-inviscid 2D dynamics. Experimentally, these meta-equilibria appear to last "forever" ($\gtrsim$1 sec), i.e., until plasma diffusive or viscous effects, not included in Eqs. (1), act to dissipate the individual vortices.

Because of these attractors, the system does not evolve ergodically, and the final state cannot be predicted from statistics alone. Nor can this system be adequately approximated as point vortices punctuated by occasional merger events: the discrete vortex motion is non-Hamiltonian due to interaction with the background vorticity. In contrast, experiments on vortex dynamics without a background have shown frequencies and instability rates closely corresponding with point vortex theory [21]. It remains to be seen how ubiquitous these crystal meta-equilibria are, and the extent to which "vortex cooling" is significant in vortex dynamics even when crystal patterns do not occur.

This work was supported by DOE Contract No. DE-FG03-85ER53199, ONR Grant No. N00014-89-J-1714, and NSF Grant No. PHY94-21318.

*Present address: MCC, 3500 W. Balcones Center Drive, Austin, TX 78759-5398.

[1] R. Kraichnan, Phys. Fluids **10**, 1417 (1967).
[2] G. Batchelor, Phys. Fluids Suppl. II **12**, 233 (1969).
[3] L. Onsager, Nuovo Cimento Suppl. **6**, 279 (1949); G. Joyce and D. Montgomery, J. Plasma Phys. **10**, 107 (1973); R. A. Smith, Phys. Rev. A **43**, 1126 (1991).
[4] D. Lynden-Bell, Mon. Not. R. Astron. Soc. **136**, 101 (1967); J. Miller, P. B. Weichman, and M. C. Cross, Phys. Rev. A **45**, 2328 (1992); R. Robert and J. Sommeria, Phys. Rev. Lett. **69**, 2776 (1992).
[5] F. P. Bretherton and D. B. Haidvogel, J. Fluid Mech. **78**, 129 (1976); W. H. Matthaus and D. Montgomery, Ann. N.Y. Acad. Sci. **357**, 203 (1980); C. E. Leith, Phys. Fluids **27**, 1388 (1984).
[6] X.-P. Huang and C. F. Driscoll, Phys. Rev. Lett. **72**, 2187 (1994).
[7] A. Roshko, AIAA J. **10**, 1349 (1976).
[8] J. C. McWilliams, J. Fluid Mech. **146**, 21 (1984); L. M. Smith and V. Yakhot, Phys. Rev. Lett. **71**, 352 (1993).
[9] G. F. Carnevale *et al.,* Phys. Rev. Lett. **66**, 2735 (1991); J. B. Weiss and J. C. McWilliams, Phys. Fluids A **5**, 608 (1993).
[10] R. Benzi *et al.,* Phys. Fluids A **4**, 1036 (1992).
[11] D. G. Dritschell, Phys. Fluids A **5**, 984 (1993).
[12] P. Tabeling *et al.,* Phys. Rev. Lett. **67**, 3772 (1991); O. Cardoso *et al.,* Phys. Rev. E **49**, 454 (1994).
[13] E. J. Yarmchuk *et al.,* Phys. Rev. Lett. **43**, 214 (1979); L. J. Campbell and R. M. Ziff, Phys. Rev. B **20**, 1886 (1979).
[14] W. G. Flynn (to be published).
[15] R. J. Briggs, J. D. Daugherty, and R. H. Levy, Phys. Fluids **13**, 421 (1970); T. B. Mitchell and C. F. Driscoll, Phys. Rev. Lett. **73**, 2196 (1994); N. S. Pillai and R. W. Gould, Phys. Rev. Lett. **73**, 2849 (1994).
[16] C. F. Driscoll and K. S. Fine, Phys. Fluids B **2**, 1359 (1990); in *Non-Neutral Plasma Physics II,* edited by J. Fajans and D. H. Dubin, AIP Conf. Proc. No. 331, (AIP, New York, to be published).
[17] C. F. Driscoll, J. H. Malmberg, and K. S. Fine, Phys. Rev. Lett. **60**, 1290 (1988).
[18] A. J. Peurrung and J. Fajans, Phys. Fluids B **5**, 4295 (1993).
[19] J. C. McWilliams, J. Fluid Mech. **219**, 361 (1990).
[20] X.-P. Huang, K. S. Fine, and C. F. Driscoll, (to be published).
[21] T. B. Mitchell, C. F. Driscoll, and K. S. Fine, Phys. Rev. Lett. **71**, 1371 (1993).

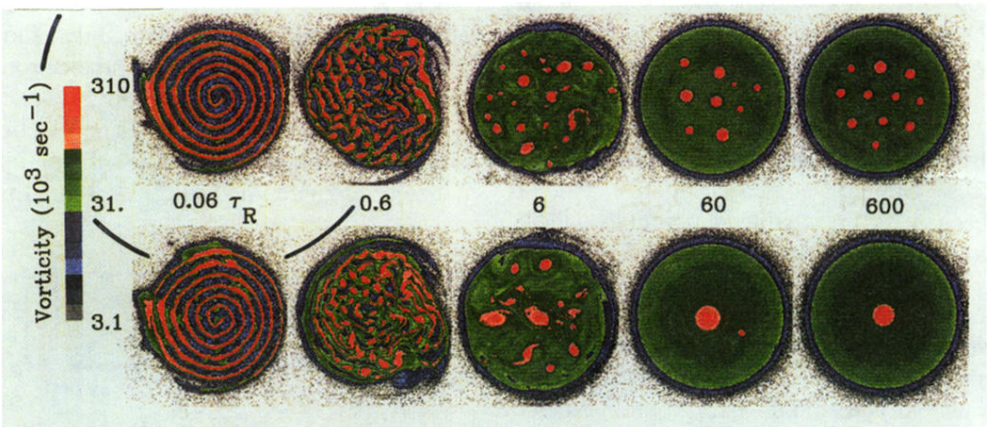

FIG. 2(color). Images of vorticity at five times for two sequences from similar initial conditions. The black arcs indicate the wall radius.

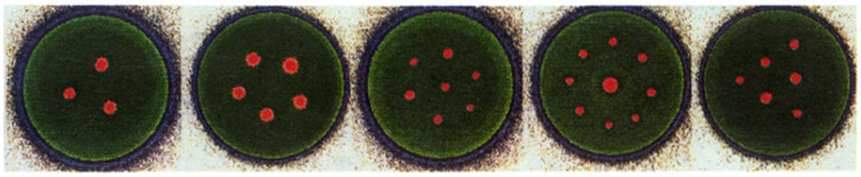

FIG. 6(color). Selection of vortex crystal patterns obtained from initial conditions similar to those of Fig. 2.